Computational Materials Science 122 (2016) 219–228

Contents lists available at ScienceDirect

Computational Materials Science

journal homepage: www.elsevier.com/locate/commatsci

Modelling the coupling between hydrogen diffusion and the mechanical behaviour of metals

O. Barrera [a,*], E. Tarleton [b,*], H.W. Tang [c], A.C.F. Cocks [a]

[a] Department of Engineering Science, University of Oxford, Parks Road, OX1 3PJ Oxford, United Kingdom
[b] Department of Materials, University of Oxford, Parks Road, OX1 3PH Oxford, United Kingdom
[c] Department of Mechanical Engineering, National Cheng Kung University, No. 1, University Rd., Tainan 701, Taiwan

ARTICLE INFO

Article history:
Received 8 February 2016
Received in revised form 23 May 2016
Accepted 24 May 2016
Available online 5 June 2016

Keywords:
Hydrogen embrittlement
Hydrogen diffusion equation
Analogy thermal/diffusion models
Finite element method
HELP mechanism
Abaqus

ABSTRACT

It is well known that hydrogen can have a detrimental effect on the mechanical properties of metals. The aim here is to provide a fully coupled model of the HELP (Hydrogen Enhanced Local Plasticity) mechanism with hydrogen transport. Using the similarities between the heat and mass diffusion equations, a coupled temperature–displacement procedure has been adopted to allow the coupling between hydrogen diffusion and the mechanical behaviour of the material to be simulated. The diffusion equation takes into account the fact that hydrogen atoms reside in interstitial sites and in trapping sites such as dislocations. In the simulations presented here it is assumed that concentration of hydrogen at the dislocations is in equilibrium with the concentration in the matrix interstitial sites. The mechanical behaviour of the material is represented by an isotropic hardening law in which the flow stress decreases with increasing hydrogen content in the matrix which is evaluated by solving the fully coupled mechanical diffusion equations. We use the model to analyse the response of a plane strain component which contains deep and sharp doubled-edged notches. For highly constrained components of this type the hydrostatic component of stress scales with the local yield strength of the material. A high local hydrostatic stress would result in a high hydrogen concentration, but a high hydrogen concentration results in softening, i.e. a low yield strength, and therefore a low hydrostatic stress. These conflicting relationships result in a balance being achieved between hydrostatic stress, hydrogen concentration and yield strength, i.e. the response does not become unstable. Also there is a high degree of kinematic determinacy in the way which the component deforms, i.e. the strain pattern in the presence of hydrogen is very similar to that when there is no hydrogen. A consequence of these two effects is that softening of the constitutive response due to the presence of hydrogen, does not lead to localization of strain and a macroscopic brittle response. Softening must be combined with other degradation process for the material to embrittle.

1. Introduction

Experimental studies and fractography analysis of iron and steels indicate a deleterious influence of hydrogen on their mechanical properties. There is extensive evidence documented in the literature on the effect of hydrogen in degrading the properties of high strength steel; resulting in reduced ductility, strength and toughness, accompanied in most cases by intergranular brittle fracture [1–4]. However, opinion is divided concerning the mechanisms that are responsible for this embrittlement. Numerous theories have been suggested and reviewed. For non hydride forming materials they can be grouped into two main primary mechanisms: hydrogen induced decohesion (HID) and hydrogen enhanced local plasticity (HELP). The HID mechanism finds its roots in the work by Scott and Troiano [1] and Oriani and Josephic [5] which postulates that hydrogen, which accumulates at a crack tip, reduces the cohesive strength of atomic bonds giving rise to a reduced fracture toughness. The HID theory has been generalized by assuming that hydrogen lowers the cohesive strength of a range of internal interfaces such as grain boundaries or carbide–matrix interfaces. The HELP mechanism implies that hydrogen enhances the dislocation mobility by reducing the elastic interaction energy between dislocations. As a consequence, hydrogen reduces the applied stress necessary to move a dislocation through a field of obstacles. This phenomenon promotes material softening. It is worth mentioning that the HID mechanism at the atomic level, i.e. hydrogen decreasing the atomic cohesion, has not been proved experimentally. However, atomistic simulations have revealed that

* Corresponding authors.
E-mail addresses: olga.barrera@eng.ox.ac.uk (O. Barrera), edmund.tarleton@materials.ox.ac.uk (E. Tarleton).

http://dx.doi.org/10.1016/j.commatsci.2016.05.030
0927-0256/

the atomic cohesion decreases with increasing hydrogen content. There have been experimental studies of the effect of hydrogen on the crack tip opening angle, which reduces with increasing hydrogen content for a Si-doped iron single crystal. The crack tip becomes sharper in the presence of hydrogen and the fracture surface appears brittle [6]. The HELP mechanism is supported by the experimental studies of Robertson using an in situ charging cell in an environmental TEM [7], in which it is shown that hydrogen enhances the dislocation mobility in stainless steel. However, recent theories recognise that the HID and HELP mechanisms might act in synergy. Novak et al. [8] present work on hydrogen-induced intergranular failure in AISI 4340 steel, in which they assume that failure initiates by decohesion at grain-boundary carbides. Hydrogen promotes the mobility of dislocations that pile up at the matrix carbide interface and enhancing the local stress there. Recently, the authors [9–11] have modelled the behaviour of a carbide-rich region in a dissimilar weld interface in the presence of hydrogen. This carbide rich region provides a low energy path for crack growth. An Abaqus finite element model of the carbide-rich microstructure was created by image processing which converts a TEM image into a finite element mesh. The presence of fine carbides plays an important role in the constitutive response of these materials. Simulations show that in regions where the hydrogen content is high the matrix surrounding the carbides softens and plastic flow is localized. Moreover, the presence of hydrogen lowers the cohesive strength, giving rise to microcrack formation at the carbide–matrix interface, leading to microvoid formation. As deformation proceeds the pores enlarge and link to form cracks, which generates the failure surface. This failure process is supported by experimental observation of failed components.

In order to fully model these and other failure mechanisms that have been proposed in the literature we need to solve the hydrogen diffusion equation to determine how hydrogen is distributed inside the material and couple this with the mechanical constitutive response of the material. The aim of this paper is to explain in details how to solve coupled hydrogen diffusion-mechanics problems in a finite element context by using the commercial finite element software Abaqus. We use the similarity between heat transport and diffusion in order to adopt the coupled tempera ture–displacement procedure available in Abaqus to effectively solve diffusion-mechanics problems. This requires the implementation of a user subroutine (UMATHT) for the diffusion equation. Here we concentrate on coupling the elasto-plastic response with models of diffusional transport and use the resulting routines to analyse a range of problems that have been designed to provide new insights into the HELP mechanism. In a subsequent paper we combine these routines with those for interface decohesion, modelled using cohesive elements, to model situations where diffusion, plastic deformation and decohesion (e.g. at grain boundaries or carbide/matrix interfaces) combine to determine the component response.

The structure of this paper is as follows. Firstly, we give a detailed description of the hydrogen diffusion equation. We then discuss the analogy with the heat transfer problem and the implementation of the equation in a UMATHT subroutine in Abaqus. We include details of the implementation. We solve first a simple diffusion problem for which an analytic solution is available, and then analyse diffusion in an elastic plate with a hole and compare the solution with analytical results. Both these simulations serve to validate the models and the code. We then analyse the response of a double-edged notched plane strain component whose isotropic hardening law is a function of the hydrogen content. We show the effect of plastic strain on the concentration of hydrogen in the traps and in the lattice and evaluate whether for this type of component plastic flow localizes, leading to failure at low macroscopic plastic strain, i.e. whether failure can occur exclusively by a HELP process.

2. Hydrogen diffusion equation

It is well known that hydrogen being the smallest element diffuses more easily through metals than any other element. Even at low concentration, hydrogen often leads to the embrittlement of metals for reasons that are not yet well understood, but are certainly related to the speed at which it can diffuse to highly stressed regions. Hydrogen atoms move through a metal by normal interstitial site (NILS) diffusion or dislocation transport. Hydrogen atoms reside either at NILS or at trapping sites such as dislocations, grain boundaries, carbide/matrix interfaces, microvoids and other defects. The vast majority of sites are the NILS and the minor fraction of sites are the traps. Here we consider a lattice consisting of two kinds of sites for occupancy by hydrogen. Hydrogen trapping at defects has a large effect on the diffusion process. Hydrogen diffuses so easily that even shallow traps can produce a significant effect on the diffusivity. One of the first theories on the mobility of dissolved hydrogen in an iron lattice containing trapping sites was given by McNabb and Foster [12]. They introduced a diffusion equation solved with terms for sources and sinks. Oriani [13] reformulated the work by McNabb and Foster introducing the assumption of local equilibrium between the mobile and the trapped populations for a restricted domain of degree of trap coverage. Sofronis and McMeeking [14] formulated the hydrogen transport problem coupled with large deformation elastic–plastic behaviour of a material based on Oriani's theory. In [14] the authors incorporated the effect of hydrostatic stress and trapping sites at dislocations, which increase in number as the material deforms plastically. Krom et al. [15] demonstrated that the hydrogen transport model proposed in [14] does not provide a correct hydrogen balance. Hence in [15] a modification on the hydrogen diffusion model is introduced which includes a factor depending on the strain rate. The strain rate factor decreases the hydrogen concentration in lattice sites due to the filling of trap sites.

2.1. Implications of Oriani's assumptions

Oriani's theory is based on considering a lattice consisting of two kinds of sites for occupancy by hydrogen. He postulates that the vast majority of sites are the ordinary or "normal interstitial" sites. The minor fraction of sites called "trapping" sites provides an energetically favourable environment for occupancy by the hydrogen atoms. We consider here the case in which the number of trapping sites is small. The trap population then does not reduce significantly the cross-section for diffusion in the normal lattice. We denote the hydrogen concentration in the lattice as C_L (number of H atoms per unit volume) and use C_X to denote the concentration associated with the hydrogen in the traps. In this paper we consider only one kind of trap, i.e. hydrogen trapped at dislocations. The total concentration of hydrogen is given by $C_T = C_L + C_X$, where

$$C_L = \beta\theta_L N_L \tag{1}$$

$\beta$is the number of interstitial sites per solvent atom, $0 \leqslant \theta_L \leq 1$, is the fraction of lattice sites occupied by hydrogen atoms and

$$N_L = \frac{\rho N_A}{A_r} = \text{const.} \tag{2}$$

is the number of atoms of solvent per unit volume (atoms/m^3). The density and relative atomic mass of the lattice element are ρ and A_r respectively and N_A is Avogadro's number. Similarly C_X is the hydrogen concentration trapped at dislocations:

$$C_X = \alpha\theta_X N_X \tag{3}$$

$\alpha = 1$ denotes the number of trapping sites, N_X (atoms/m^3) denotes the number of atomic trapping sites along the total dislocation line length per unit volume, which increases with plastic strain and $0 \leqslant \theta_X \leq 1$ is the fraction of trapping sites occupied by H atoms. We assume that N_X is proportional to the dislocation density ρ^d and that the dislocation density is a function of the accumulated plastic strain,

$$N_X(\varepsilon^p) = \frac{\sqrt{2}}{a}\rho^d(\varepsilon^p) \tag{4}$$

where a is the lattice constant and the prefactor is $1/b$, where b is the magnitude of the $a/2\langle 1\,1\,0\rangle$ Burgers vector in fcc which is a reasonable approximation for the atomic spacing along a dislocation line. We discuss particular forms of $\rho^d(\varepsilon^p)$ in Section 4.

It proves more convenient when analysing H diffusion in a body to express the concentration in units of mol/m^3. We place a bar over the symbol when dealing with molar quantities, i.e.:

$$\bar{C}_L = \frac{C_L}{N_A} \tag{5}$$

$$\bar{C}_X = \frac{C_X}{N_A} \tag{6}$$

Mass conservation states that the rate of change of the total hydrogen concentration in a volume Ω is equal to the flux $\bar{\mathbf{J}}$ (mol m^{-2} s^{-1}) through the surface $\partial\Omega$.

$$\frac{\partial}{\partial t}\int_\Omega (\bar{C}_L + \bar{C}_X)d\Omega + \int_{\partial\Omega}\bar{\mathbf{J}}\cdot\mathbf{n}dS = 0 \tag{7}$$

where n is the outward normal to $\partial\Omega$. The driving force for diffusion is the chemical potential gradient, the flux $\bar{\mathbf{J}}$ can be expressed as follows:

$$\bar{\mathbf{J}} = -\frac{D_L\bar{C}_L}{RT}\nabla\mu \tag{8}$$

where D_L is the diffusion coefficient for hydrogen. Here we ignore pipe diffusion along the dislocation line [16] on grounds that the dislocation spacing is much larger than the core radius and that fast' pipe diffusion may be slower than diffusion through the lattice [17]. The chemical potential, μ, is defined as follows:

$$\mu = \mu_0 + RT\ln\bar{C}_L + \mu_\sigma \tag{9}$$

μ_0 represents the chemical potential at standard condition, $\mu_\sigma = -\sigma_H V_H$ where σ_H is the hydrostatic stress and $\bar{V}_H$ the partial molar volume of hydrogen. Substituting (9) into (8) we obtain:

$$\bar{\mathbf{J}} = \frac{D_L V_H\bar{C}_L}{RT}\nabla\sigma_H - D_L\nabla\bar{C}_L \tag{10}$$

Substituting (10) into (7) then gives:

$$\frac{\partial}{\partial t}\int_\Omega (\bar{C}_L + \bar{C}_X)d\Omega + \int_{\partial\Omega}\left(\frac{D_L V_H\bar{C}_L}{RT}\nabla\sigma_H - D_L\nabla\bar{C}_L\right)\cdot\mathbf{n}dS = 0 \tag{11}$$

Applying the divergence theorem, we obtain:

$$\frac{\partial\bar{C}_L}{\partial t} + \frac{\partial\bar{C}_X}{\partial t} + \nabla\cdot\left(\frac{D_L V_H\bar{C}_L}{RT}\nabla\sigma_H\right) - \nabla\cdot(D_L\nabla\bar{C}_L) = 0 \tag{12}$$

In Eq. (12) there are two unknowns: $\bar{C}_L$ and $\bar{C}_X$. However following Oriani's theory the H concentration in the lattice was assumed to be in equilibrium with the concentration in the traps. This means that once we know the concentration in the lattice we can calculate the concentration in the traps.[1]

$$\bar{C}_X = \frac{N_X\theta_X}{N_A} = \frac{N_X}{N_A}\frac{1}{1+\frac{(1-\theta_X)}{\theta_X}} \tag{13}$$

Oriani's theory [13] states that for $\theta_L \ll 1$:

$$\frac{\theta_X}{(1-\theta_X)} = K\theta_L \tag{14}$$

where

$$K = \exp\left(\frac{-W_B}{RT}\right) = \text{const.} \tag{15}$$

and $W_B < 0$ represents the binding energy for the traps. Substituting (14) into (13) we can express the concentration in the traps as a function of the density of trapping sites and the concentration in the lattice:

$$\bar{C}_X(C_L,\bar{N}_X) = \bar{N}_X(\varepsilon^p)\frac{K\theta_L}{1+K\theta_L}\frac{\beta\bar{N}_L}{\beta\bar{N}_L} = \bar{N}_X(\varepsilon^p)\frac{K\bar{C}_L}{\beta\bar{N}_L + K\bar{C}_L} \tag{16}$$

where

$$\bar{N}_L = \frac{N_L}{N_A} = \text{const.} \quad \bar{N}_X(\varepsilon^p) = \frac{N_X(\varepsilon^p)}{N_A}. \tag{17}$$

where ε^p is a scalar measure of the plastic strain and $\bar{N}_X(\varepsilon^p)$ is a function of the plastic strain through (4) and the constitutive relationship that relates dislocation density to ϵ^p. The time derivative of the trapping site concentration, $\partial\bar{C}_X/\partial t$ in (12),can now be expressed as follows:

$$\frac{\partial\bar{C}_X}{\partial t} = \frac{\partial\bar{C}_X}{\partial\bar{C}_L}\frac{\partial\bar{C}_L}{\partial t} + \frac{\partial\bar{C}_X}{\partial\bar{N}_X}\frac{d\bar{N}_X}{d\varepsilon^p}\frac{d\varepsilon^p}{dt} \tag{18}$$

Substituting (18) in (12) we obtain:

$$\frac{\partial\bar{C}_L}{\partial t}\left(1+\frac{\partial\bar{C}_X}{\partial\bar{C}_L}\right) - \nabla\cdot(D_L\nabla\bar{C}_L) + \nabla\cdot\left(\frac{D_L\bar{C}_L V_H}{RT}\nabla\sigma_H\right) + \frac{\partial\bar{C}_X}{\partial\bar{N}_X}\frac{d\bar{N}_X}{d\varepsilon^p}\frac{d\varepsilon^p}{dt} = 0 \tag{19}$$

From (16) we obtain:

$$\frac{\partial\bar{C}_X}{\partial\bar{C}_L} = \frac{\beta\bar{N}_X K\bar{N}_L}{(\beta\bar{N}_L + K\bar{C}_L)^2} \tag{20}$$

$$\frac{\partial\bar{C}_X}{\partial N_X} = \frac{K\bar{C}_L}{(\beta\bar{N}_L + K\bar{C}_L)} \tag{21}$$

3. Analogy with the heat transfer problem

In order to implement the coupled hydrogen transport equation given in Eqs. (19)–(21) we use the similarities with the heat equation as noted by Oh et al. [19]. Table 1 summarizes the analogy between the heat equation and the hydrogen diffusion equation. It can be seen that the form of the equations are identical. The degree of freedom in the heat equation is temperature, T, whereas in the hydrogen diffusion equation it is $\bar{C}_L$. We believe that there is a mistake in the table in which Oh et al. [19] summarize the analogy of variables between the heat transfer analysis within Abaqus and the hydrogen diffusion analysis. We refer in particular to the definition of the variable that is analogous to the internal energy U_q in Table 1 which is the total hydrogen concentration $\bar{C}_T$ and not the chemical potential as claimed by Oh et al. The coupled thermo-mechanics procedure (available in Abaqus) can then be used to solve coupled diffusion-mechanics problems. In Oh et al. [19] the evaluation of the gradient of hydrostatic stress inside an element is calculated by storing the hydrostatic stress (evaluated at each gauss point) in an external file which is then read inside

[1] This contradicts Eq. (16) in [18] which is dimensionally inconsistent.

Table 1
Analogy of variables between heat transfer and diffusion analysis in ABAQUS.

Heat equation	Mass diffusion equation
$\rho c_P \frac{\partial T}{\partial t} + \nabla \cdot \mathbf{J}_q + r_q = 0$	$\frac{C_T}{\partial t} + \nabla \cdot \mathbf{J}_m + r_m = 0$
Derivative of thermal energy per unit mass $\dot{U}_q = c_P \frac{\partial T}{\partial t}$	Derivative of total H concentration $\frac{\partial C_T}{\partial t} = \frac{\partial (\bar{C}_L + \bar{C}_X)}{\partial t}$
Degree of freedom: temperature T	Degree of freedom: lattice H concentration $\bar{C}_L$
Heat flux: $\vec{\mathbf{J}}_q$	Hydrogen flux: $\vec{\mathbf{J}}_m = \frac{D_L \bar{C}_L V_H}{RT} \nabla \sigma_H - D_L \vec{\nabla} \bar{C}_L$
Heat source: r_q (assume $r_q = 0$)	Hydrogen source: r_m (assume $r_m = 0$)
density: ρ	1 Unity

Table 2
Quantities that need to defined in the UMATHT subroutine.

Heat equation	Mass diffusion equation
Quantity to be defined in the UMATHT $\frac{\partial U_q}{\partial T}; \frac{\partial U_q}{\partial \nabla T}; \frac{\partial \vec{\mathbf{J}}_q}{\partial T}; \frac{\partial \vec{\mathbf{J}}_q}{\partial \nabla T}$	Quantity to be defined in the UMATHT $\frac{\partial C_T}{\partial \bar{C}_L}; \frac{\partial C_T}{\partial \bar{N}_X}; \frac{\partial \vec{\mathbf{J}}_m}{\partial \bar{C}_L}; \frac{\partial \vec{\mathbf{J}}_m}{\partial (\nabla \bar{C}_L)}$

the user material routine for the implementation of the mechanical constitutive law (UMAT) to be then passed to the UMATHT subroutine, which implements the thermal constitutive model. Here we show that we can compute directly the gradient of hydrostatic stress inside the UMATHT by using a commonblock with Abaqus USDFLD and GETVRM subroutines. Here we report all the details necessary to fully implement the procedure.

3.1. Implementation of the model in the UMATHT subroutine

The thermal constitutive behaviour of the material and internal heat generation during heat transfer can be defined by the variation of internal energy with temperature and with spatial temperature gradient i.e. $\frac{\partial U_q}{\partial T}; \frac{\partial U_q}{\partial \nabla T}$ in the UMATHT subroutine available in Abaqus. The analogous quantities for the diffusion problem are summarized in Table 2. It is essential to note that in order to implement the hydrogen diffusion equation, the quantities to be defined are: the variation of total hydrogen concentration ($\bar{C}_T = \bar{C}_L + \bar{C}_X$) with $\bar{C}_L$ and with the trap density $N_X(\varepsilon^p)$ which is a function of plastic strain. Moreover, the variation of heat flux with temperature and with spatial temperature gradient i.e. $\frac{\partial \vec{\mathbf{J}}_q}{\partial T}; \frac{\partial \vec{\mathbf{J}}_q}{\partial (\nabla T)}$ respectively corresponds to the variation of hydrogen flux with $\bar{C}_L$ and with the hydrogen concentration gradient i.e. $\frac{\partial \vec{\mathbf{J}}_m}{\partial \bar{C}_L}; \frac{\partial \vec{\mathbf{J}}_m}{\partial (\nabla \bar{C}_L)}$. The hydrogen diffusion Eq. (19) can be written using the formalism appropriate for the subroutine as follows:

$$\bar{C}_T(t + \Delta t) = \bar{C}_T(t) + \frac{\partial \bar{C}_T}{\partial \bar{C}_L} d\bar{C}_L + \frac{\partial \bar{C}_T}{\partial \bar{N}_X} \frac{d\bar{N}_X}{d\varepsilon_p} d\varepsilon_p \tag{22}$$

The terms in (22) can be obtained as follows:

$$\begin{aligned} &\frac{\partial \bar{C}_T}{\partial \bar{C}_L} = 1 + \frac{\beta \bar{N}_X K \bar{N}_L}{(\beta \bar{N}_L + K \bar{C}_L)^2} \\ &\frac{\partial \bar{C}_T}{\partial \bar{N}_X} = \frac{K \bar{C}_L}{K \bar{C}_L + \beta \bar{N}_L} \\ &\frac{\partial \vec{\mathbf{J}}_m}{\partial \bar{C}_L} = \frac{D_L V_H}{RT} \vec{\nabla} \sigma_H \\ &\frac{\partial \vec{\mathbf{J}}_m}{\partial (\nabla \bar{C}_L)} = -D_L \mathbf{I} \end{aligned} \tag{23}$$

where $\mathbf{I}$ is the identity matrix. It is essential to note that in order to calculate the gradient of hydrostatic stress $\nabla \sigma_H$ in Eq. (23) we need to use a commonblock together with the USDFLD subroutine. USDFLD allows field variables at a material point to be defined as a function of time or of any of the available material point quantities; in this case the direct components of stress. USDFLD calls the utility routine GETVRM to provide access to the values of the material point quantities at the start of the increment. In order to evaluate the gradient of hydrostatic stress we interpolate the hydrostatic stress inside the element at each gauss point. The interpolation is identical to the procedure used to calculate the strain field from the nodal displacements. Here we interpolate from the gauss points. 4 – node coupled temperature–displacement plane strain elements CPE4T cannot be used for this purpose as they are linear elements for which Abaqus imposes a constant hydrostatic stress within the element. Here we use quadratic 8 – node hybrid coupled tem perature–displacement plane strain elements CPE8HT. Then

$$\begin{aligned} \nabla \sigma_H = \frac{\partial \sigma_H}{\partial x_j} &= \left[\frac{\partial \sigma_H}{\partial s_1} \frac{\partial s_1}{\partial x_1} + \frac{\partial \sigma_H}{\partial s_2} \frac{\partial s_2}{\partial x_1}, \frac{\partial \sigma_H}{\partial s_1} \frac{\partial s_1}{\partial x_2} + \frac{\partial \sigma_H}{\partial s_2} \frac{\partial s_2}{\partial x_2} \right] \\ &= \left[\frac{\partial \sigma_H}{\partial s_1}, \frac{\partial \sigma_H}{\partial s_2} \right] \begin{bmatrix} \frac{\partial s_1}{\partial x_1} & \frac{\partial s_1}{\partial x_2} \\ \frac{\partial s_2}{\partial x_1} & \frac{\partial s_2}{\partial x_2} \end{bmatrix} = \frac{\partial \sigma_H}{\partial s_i} J_{ij}^{-1} \end{aligned} \tag{24}$$

$$\begin{aligned} &\frac{\partial \sigma_H}{\partial s_i} = \sum_a \frac{\partial N^a}{\partial s_i} \sigma_H^a, \quad J_{ij}^{-1} = \left(\frac{\partial x_1}{\partial s_1} \frac{\partial x_2}{\partial s_2} - \frac{\partial x_2}{\partial s_1} \frac{\partial x_1}{\partial s_2} \right)^{-1} \begin{bmatrix} \frac{\partial x_2}{\partial s_2} & -\frac{\partial x_1}{\partial s_2} \\ -\frac{\partial x_2}{\partial s_1} & \frac{\partial x_1}{\partial s_1} \end{bmatrix}, \\ &\frac{\partial x_i}{\partial s_j} = \sum_a \frac{\partial N^a}{\partial s_j} X_i^a \end{aligned} \tag{25}$$

where the values at node $a = 1 \ldots 9$, X^a and σ^a, are the integration point values of the parent element as the element is considered to be a 9 node element whose nodes coincide with the gauss points of the fully integrated 8 node element. The shape function derivatives are evaluated at the node, that is to say the gradient can vary within an element due to changes in shape of the element, captured by the inverse of the Jacobian and variations in σ_H.

4. Numerical results

In this section we analyse three problems with increasing degree of complexity. We start by analysing a 1D diffusion problem, which allows the numerical simulation to be compared directly with an analytical solution. We then analyse an elastic diffusion 2D problem in the absence of traps, for which analytical results are available to verify the accuracy of the steady state solution at constant load. We then analyse a fully coupled elasto-plastic diffusion problem and evaluate the HELP mechanism of H embrittlement described in the introduction.

4.1. Pure diffusion

We present here the solution of a simple 1D diffusion problem, Fig. 1, which we can compare with the analytical solution. We consider that all H resides in lattice sites, i.e there are no traps and $\bar{C}_T = \bar{C}_L$. Fig. 1 shows a bar of length l = 50 mm. $\bar{C}_L = 0$ throughout the bar and at time t = 0 the concentration at one end is increased to 100 $\frac{\text{mol}}{\text{m}^3}$. Fig. 1 shows the full transient solution. The governing equation for this problem is well known as well as the analytic solution [20]:

$$\frac{\partial \bar{C}_L^2}{\partial x^2} = \frac{1}{D_L} \frac{\partial \bar{C}_L}{\partial t} \tag{26}$$

The analytic solution reads:

$$\bar{C}_L(x,t) = \bar{C}_0 + \frac{x}{l}(\bar{C}_l - \bar{C}_0) + \sum_{n=1}^{\infty} c_n \exp\left(-\frac{n^2 \pi^2 D_L t}{l^2} \right) \sin\left(\frac{n \pi x}{l} \right) \tag{27}$$

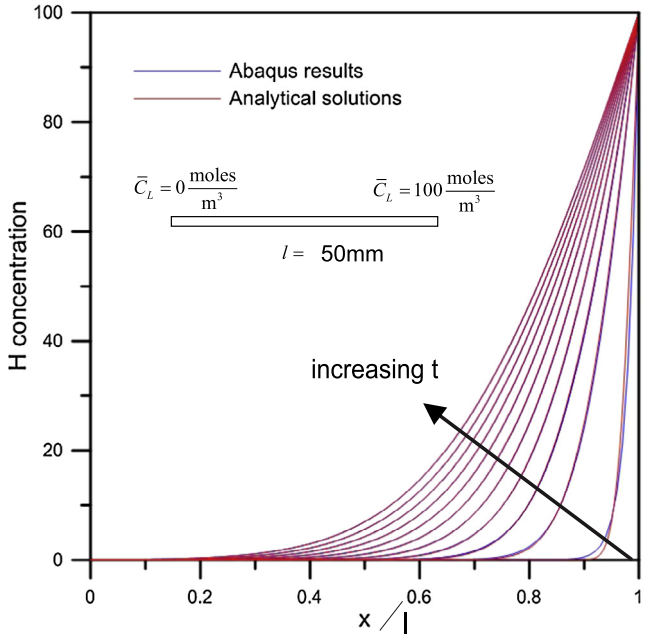

Fig. 1. Transient concentration of H considering no trapped species:comparison between analytic solution and simulation.

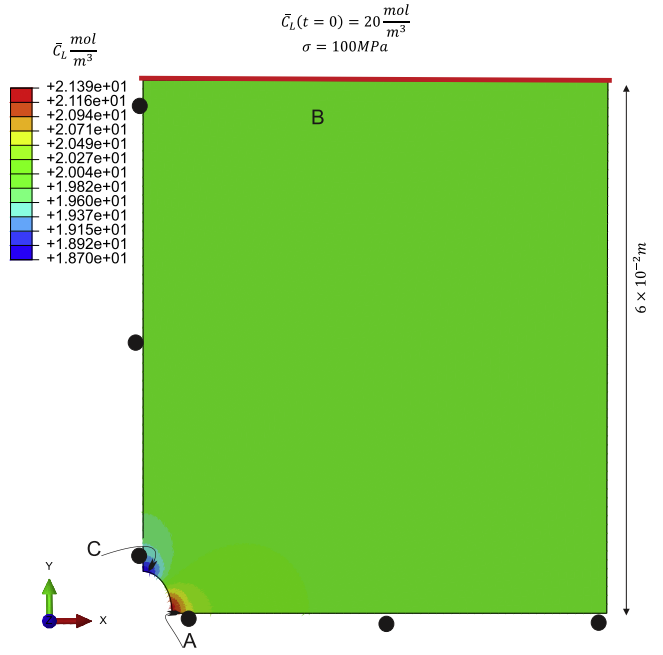

Fig. 2. Concentration of H considering no trapped species:comparison between analytic solution $\bar{C}_{LA} = 21.4$ and simulation $\bar{C}_{LA} = 21.39$.

and

$$c_n = \frac{2}{l}\int_0^l f(x)\sin\left(\frac{n\pi x}{l}\right)dx + \frac{2}{n\pi}\left[-1^n(\bar{C}_l - \bar{C}_0)\right] \tag{28}$$

Eq. (26) is essentially a simplified version of (19) in which the term $\frac{\partial \bar{C}_X}{\partial \bar{C}_L} = 0$ and the last two terms of (19) are zero. Eq. (26) is implemented in UMATHT by simply coding the following terms:

$$\frac{\partial \bar{C}_T}{\partial \bar{C}_L} = 1 \tag{29}$$

$$\frac{\partial \bar{\mathbf{J}}_m}{\partial(\nabla \bar{C}_L)} = -D_L\mathbf{I} \tag{30}$$

Fig. 1 shows the transient hydrogen concentration distribution along the bar for both the analytical and computational solution. The value of diffusivity is $D_L = 3.8 \times 10^{-11}$ m^2/s and the computations were conducted using quadratic continuum coupled tempera ture–displacements hybrid element i.e. CPE8HT. The characteristic time for diffusion (i.e. time necessary for hydrogen to diffuse along the bar) can be determined by using the well known relation $t = \frac{l^2}{D_L} = 6.5 \times 10^7$ s. Here we consider a fixed time step of $dt = 1 \times 10^4$ s and a total time of $t = 1 \times 10^6$ s. The Abaqus results almost perfectly agree with the analytic solution of (27).

4.2. Coupled diffusion-mechanics problems

This section aims to validate our code with analytical solutions for more complex geometries. We present numerical results for a plate with a hole and a plate with deep double-edged notch. In both cases we assume that the hydrogen concentration is initially uniform in the plates. We then ramp up the displacement remote from the discontinuities. The aim is to predict how the hydrogen redistributes inside the plate. Furthermore we assume that all boundaries are insulated so that there is no flux of hydrogen away from the plate.

4.2.1. Elastic plate with a hole

In the first example we consider an elastic plate in which we consider that all hydrogen resides in lattice sites, i.e. we don't consider trapped hydrogen and $\bar{C}_L = \bar{C}_T$. We present here a comparison with an analytic solution. The aim is to calculate the H concentration at the edge of the hole. The example in Fig. 2 illustrates a plate with a hole subjected to a uniform stress $\sigma_y = 100$ Pa. The hydrogen concentration in the lattice is initially $\bar{C}_L = 20$ mol m^{-3} throughout the plate. The plate is modelled with continuum quadratic hybrid elements (CPE8HT) with Young's modulus 200 GPa and Poisson's ratio $\nu = 0.3$. The last two equations of (23) give the diffusional response. In the simulations presented here we have used $D_L = 3.8 \times 10^{-11}$ m^2 s and $V_H = 2 \times 10^{-6}$ m^3 mol. The characteristic time for diffusion is $t = l^2/D_L = 4.2 \times 10^5$ s where $l = 4 \times 10^3$ m is equal to the radius of the hole. Here we consider a total time of $t = 1 \times 10^{10}$ s and a time step which varies between $dt = 100$ s and $dt = 1000$ s. In this case Abaqus requires the value of the maximum change in concentration at each increment to be specified. This is indicated by a variable called *deltmx*. It is worth noting that this variable needs to be an integer and its minimum value is *deltmx* = 1 mol m^{-3} which is the value that we use here. Over the timescale of the simulations the hydrogen completely redistributes and a state of equilibrium is achieved, i.e. the chemical potential μ is uniform throughout the plate. We concentrate on this equilibrated state here, because it allows us to compare the computations directly with analytical expressions. Consider location A and B of Fig. 2, where A is at the surface of the hole where it meets the x-axis and B is remote from the hole, where the stress is uniform and equal to the applied stress. The chemical potential at these two locations (see Eq. (9)) is given by:

$$\mu_A = \mu_0 + RT\ln\bar{C}_{LA} - \sigma_A V_H \tag{31}$$

$$\mu_B = \mu_0 + RT\ln\bar{C}_{LB} - \sigma_B V_H \tag{32}$$

where the superscripts A and B refer to locations A and B of Fig. 2 $\sigma_B = 100(1+\nu)/3 = 43.3$ MPa are equal to the local hydrostatic component of stress. The hole is small enough to consider that $\bar{C}_L$ remains equal to the initial value of 20 mol m^{-3} along the top

horizontal edge of the simulation domain. At equilibrium $\mu_A = \mu_B$. By equating (31) and (32) and noting that $\sigma_A = 130$ MPa we obtain $\bar{C}_{LA} = 1.07 \times \bar{C}_L = 21.4$. We obtain a value of $\bar{C}_{LA} = 21.39$ from the computations which is very close to the analytical solution. It is also worth mentioning that the distribution of hydrogen concentration $\bar{C}_L$ follows the distribution of hydrostatic stress which has its maximum and minimum values at A and C respectively.

4.2.2. Elastic–plastic plate with a deep notch

Here we consider a plane strain plate with deep double-edged notches as shown in Fig. 3 which shows a quarter of the plate. The plate is manufactured from an elasto-plastic material; in the analysis presented here we assume full coupling between the mechanical and diffusion processes and make constitutive assumptions that are appropriate for a Nickel based alloy. The main reason for analysing this geometry is that it gives rise to a high degree of plastic constraint, with high level of hydrostatic stress generated across the minimum section. We explore the effect of this constraint on the coupled diffusion and plastic deformation processes and evaluate whether localization of plastic flow can occur and give rise to a HELP embrittlement mechanism. We assume that the hydrogen concentration in the lattice is initially uniform throughout the plate, i.e. $\bar{C}_L = 27$ mol m^{-3} (this corresponds to about 1000 appm and 17.2 wppm) which is the order of concentrations at which embrittlement of nickel-base alloys is observed [21]. All boundaries are insulated. The displacement experienced by the top surface is gradually increased to a maximum value of 6×10^{-4} m, giving a net elongation of the plate of 1%. The displacement is ramped up over a time of $t = 1 \times 10^5$ s. We solve the full coupled hydrogen diffusion equation in (19) by implementing the full set of the equations in (23) in the UMATHT routine. The material parameters used in the simulations are summarized in Table 3. We consider two species of hydrogen: hydrogen in the lattice and at dislocation sites, i.e. $\bar{C}_T = \bar{C}_L + \bar{C}_L$. We are interested in predicting how the hydrogen redistributes inside the plate, both in the normal interstitial sites and at dislocations. Moreover we are interested to show the effect of plastic strain on the diffusion process. Following [22] we consider an isotropic Von Mises plasticity model in which the flow stress is a function of the hydrogen content. In particular we model the effect of hydrogen-induced material softening; this is to be viewed as an attempt to describe the experimental observations of the effect of hydrogen on dislocation mobility. We assume that the current yield strength, σ_Y, is a function of the equivalent plastic strain ε^p and $\bar{C}_L$ according to the relationship [22]:

$$\sigma_Y = \sigma_0^H \left(1 + \frac{\varepsilon^p}{\varepsilon_0}\right)^{\frac{1}{n}} \tag{33}$$

where

$$\sigma_0^H = \Psi(\bar{C}_L)\sigma_0 \tag{34}$$

where σ_0^H is the initial yield strength in the presence of hydrogen that decreases with increasing hydrogen concentration, $\epsilon_0 = \frac{\sigma_0^H}{E}$, E is Young's modulus and $\Psi(\bar{C}_L)$ is a monotonically decreasing function of hydrogen concentration at NILS. We further assume that the dislocation density, ρ^d, depends on the accumulated plastic strain as follows [22]:

$$\rho^d = \rho_0^d + \gamma\epsilon^p \quad \epsilon^p < 0.5 \tag{35}$$

$$\rho^d = 10^{16} \quad \epsilon^p > 0.5 \tag{36}$$

where $\rho_0^d = 10^{10}$ m^{-2} denotes the dislocation density for the annealed material and $\gamma = 2 \times 10^{16}$ m^{-2}. In the simulations presented here we either assume that $\Psi(\bar{C}_L)$ is constant or that [9]:

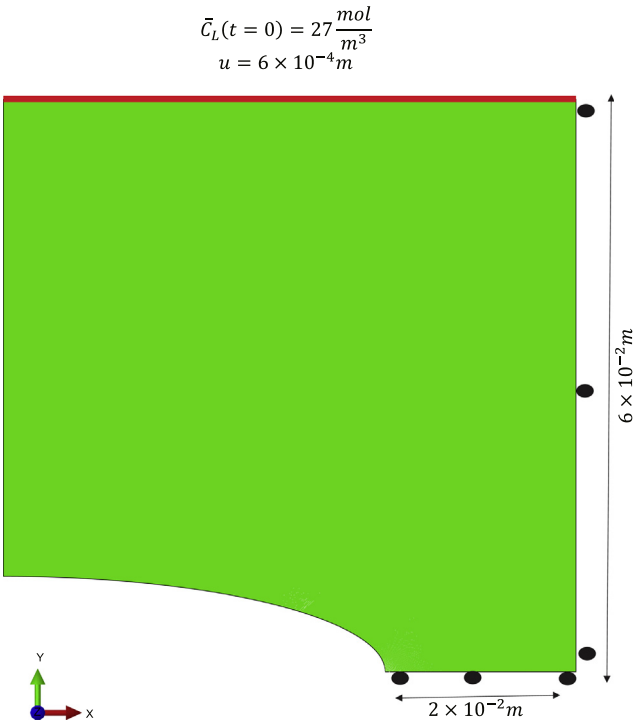

Fig. 3. Geometry and boundary conditions of the plate with a deep notch.

Table 3
Material parameters.

Parameter	Value
N_L Number of solvent atoms (Ni) per unit volume	9.24×10^{28} mol m^{-3}
N_A Avogadro's number	6.023×10^{23} atoms mol^{-1}
D_L Lattice hydrogen diffusivity	3.8×10^{-11} m^2 s^{-1}
β Number of interstitial sites per solvent (Ni) atom	6
ρ_0^d Dislocation density for the annealed material	10×10^{10} m^{-2}
a Lattice parameter	2.86×10^{-10} m
V_H Partial molar volume of hydrogen	2×10^{-6} m^3 mol^{-1}
W_B Binding energy of hydrogen to dislocations	-18 kJ mol^{-1}

$$\Psi(\bar{C}_L) = \left[1 - (1-\xi)\left(\frac{(\bar{C}_L - \bar{C}_{min})}{\bar{C}_{max} - \bar{C}_{min}}\right)\right] \tag{37}$$

where $\bar{C}_{max} = 35$ mol m^{-3} and $\bar{C}_{min} = 15$ mol m^{-3} in order to ensure that the value of the quantity $(\bar{C}_L - \bar{C}_{min})/(\bar{C}_{max} - \bar{C}_{min})$ is bounded between 0 and 1. We assume that $\xi = 0.2$. $\sigma_0 = 500$ MPa is the initial yield strength in the absence of hydrogen and $n = 5$ is the hardening exponent which is considered not to be affected by hydrogen. For simplicity, we ignore swelling due to the introduction of hydrogen into a material. The elastic properties are Young's modulus $E = 200$ GPa and Poisson's ratio $\nu = 0.3$. Eqs. (33) and (34) have been implemented in a UMAT subroutine within ABAQUS ([10,11]). We solve a coupled diffusion-mechanics problem in which the plastic strain affects the concentration of hydrogen concentration associated with the traps by enhancing the trap dislocation density N_X as seen in Eq. (3). Furthermore following Oriani's theory the hydrogen concentration in the lattice $\bar{C}_L$ is in equilibrium with the hydrogen concentration in the traps $\bar{C}_X$, hence $\bar{C}_X$ also depends on the local hydrostatic component of stress. The characteristic time for diffusion is $t = l^2/D_L = 4.2 \times 10^7$ s. The length l is the size of the notch, i.e. $l = 4 \times 10^{-2}$ m. Here we consider a total time of $t = 1 \times 10^6$ s and a fixed time step of $dt = 1 \times 10^3$ s.

4.2.3. No influence of hydrogen on the flow stress

We show first the case in which the hydrogen does not influence the plastic properties of the material i.e. in (33) the function $\Psi(\bar{C}_L)$ is constant. We want to explore the two extreme cases i.e.

(a) $\Psi(\bar{C}_L) = 1, \sigma_0^H = 1 \times \sigma_0 = 500$ MPa.

(b) $\Psi(\bar{C}_L) = 0.2, \sigma_0^H = 0.2 \times \sigma_0 = 100$ MPa.

Fig. 4 shows the stress–strain response in the y-direction (σ_y versus ϵ_y) of the material in the element immediately ahead of the notch for both (a) and (b). The plastic strain contour plot at the final increment for case (b) is also included in Fig. 4. The plastic strain distribution for case (a) is very similar although the magnitudes are lower due to the greater contribution from the elastic strains to the overall deformation arising from the higher yield strength and stress levels. The material starts yielding at the edge of the notch where the Von Mises stress is highest. Hence plastic strain develops first at the notch root and then spreads to the centre of the plate. The plastic strain at the notch root is slightly higher in case (b), i.e. $\epsilon^p = 15.8\%$, than case (a), where it reaches a value of $\epsilon^p = 14.2\%$. Fig. 5 shows the distribution of the hydrostatic component of stress ahead of the notch for the two cases. The hydrostatic stress has a peak at about 0.0036 m from the notch root for both cases, with the magnitude scaling with the local yield strength of the material. Fig. 6 shows the corresponding distributions of $\bar{C}_L$ ahead of the notch, which peaks at $\bar{C}_L = 30.4$ mol m^{-3} and $\bar{C}_L = 28.4$ mol m^{-3} for cases (a) and (b) respectively. $\bar{C}_L$ is higher in case (a) due to the higher hydrostatic stress. The $\bar{C}_X$ distributions for cases (a) and (b) are shown in Fig. 7. The hydrogen concentration associated with the dislocation traps $\bar{C}_X$ is localized in the region of high plastic strain i.e. it follows the distribution of plastic strain shown in Fig. 4. Now the amount of hydrogen in the traps is higher for the low yield strength material due to the higher level of inelastic strain close to the notch root.

4.2.4. Influence of hydrogen on the flow stress

We now consider the situation where $\Psi(\bar{C}_L)$ is a function of hydrogen concentration according to the relationship of Eq. (37). This relationship is bounded by the two conditions (a) and (b) considered above and the results for these simpler problems provide a useful context to evaluate the results for this more complicated problem. The distribution of σ_H, $\bar{C}_L$ and $\bar{C}_X$ across the minimum section are shown in Figs. 5–7 as case (c) where they can be compared directly with the solutions for the situation where the plastic properties are independent of the hydrogen content. In each case the trends are very similar, with the results lying close to those for case (b) considered above. Fig. 8 shows the distribution of $\Psi(\bar{C}_L)$ at the end of the simulation which has a minimum value of 0.354 ahead of the notch where the hydrostatic component of stress also peaks (Fig. 5) and the concentration in the lattice $\bar{C}_L$ riches its maximum value (Fig. 6). Fig. 9 shows the distribution of $\Psi(\bar{C}_L)$ ahead the notch root with increasing simulation time as the remote load is ramped up. $\Psi(\bar{C}_L)$ (and therefore the yield stress of the material) varies non-uniformly along the minimum section. As the displacement is increased the stress increases ahead of the notch root and as the material deforms plastically the hydrostatic stress and therefore $\bar{C}_L$ increases. This increase in $\bar{C}_L$ promotes softening of the material, but this is offset by the strain hardening (see (33)), so there is a gradual net increase in the yield strength σ_Y throughout the simulation. A consequence of this is that σ_H and $\bar{C}_L$ gradually increase and $\Psi(\bar{C}_L)$ decreases throughout the simulation. Fig. 9 shows that from a distance greater than 0.01 m from the notch root $\Psi(\bar{C}_L)$ gradually increases. This in combination with

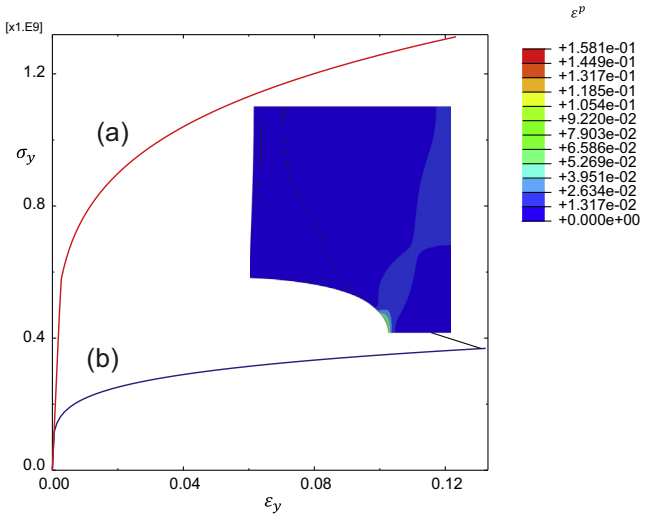

Fig. 4. Stress strain curves for (a) $\sigma_0^H = 500$ MPa and (b) $\sigma_0^H = 100$ MPa. The contour plots of plastic strain at the end of the increment for cases (b) is also included.

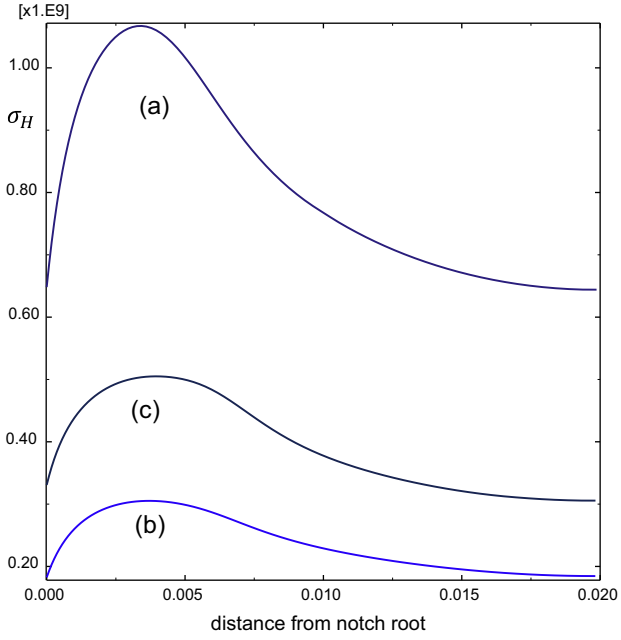

Fig. 5. Distribution of hydrostatic stress ahead of the notch root for cases (a) $\sigma_0^H = 500$ MPa, (b) $\sigma_0^H = 100$ MPa and (c) $\sigma_0^H = 500 \times \Psi(\bar{C}_L)$ MPa.

strain hardening leads to a net increase in the local yield strength. Fig. 10 shows the stress–strain response in the y-direction i.e. σ_y versus ϵ_y in an element ahead of the notch root together with the distribution of the plastic strain field at the end of the simulation. This plastic strain distribution is similar to those for the situations where H does not affect the yield strength of the material and the position and magnitude of the maximum strains are equivalent to those for case (b) above. Consequence of this is that the distribution of the density of traps is the same as for case (b). $\bar{C}_X$ depends on both the density of traps and $\bar{C}_L$, which is slightly higher for case (c) than case (b) due to the higher yield strength and hydrostatic stress. Therefore the distribution of $\bar{C}_X$ for case (c) in Fig. 7, lies slightly above that for case (b). This indicates that the deformation ahead of the notch is highly kinematically constrained. As the materials local to the notch root softens (compared

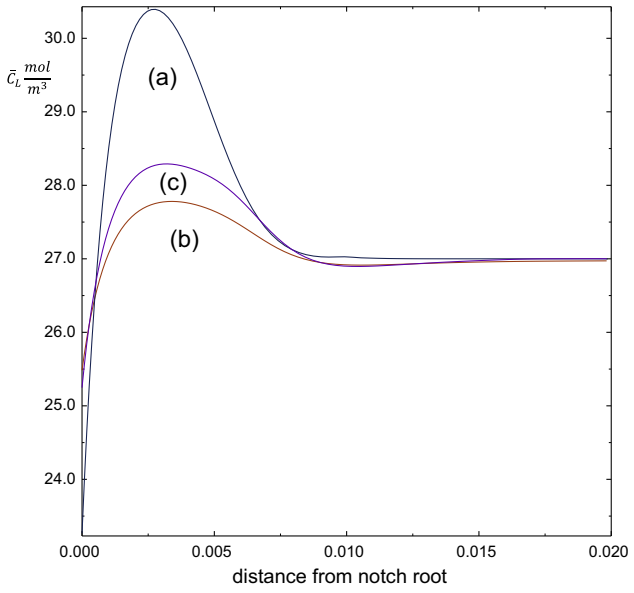

Fig. 6. H concentration in the lattice for cases (a) $\sigma_0^H = 500$ MPa, (b) $\sigma_0^H = 100$ MPa and (c) $\sigma_0^H = 500 \times \Psi(\bar{C}_L)$ MPa.

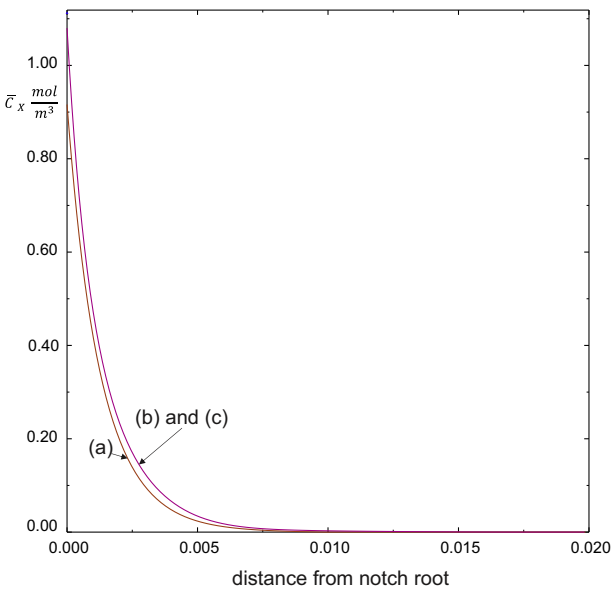

Fig. 7. H concentration in the traps for cases (a) $\sigma_0^H = 500$ MPa, (b) $\sigma_0^H = 100$ MPa and (c) $\sigma_0^H = 500 \times \Psi(\bar{C}_L)$ MPa.

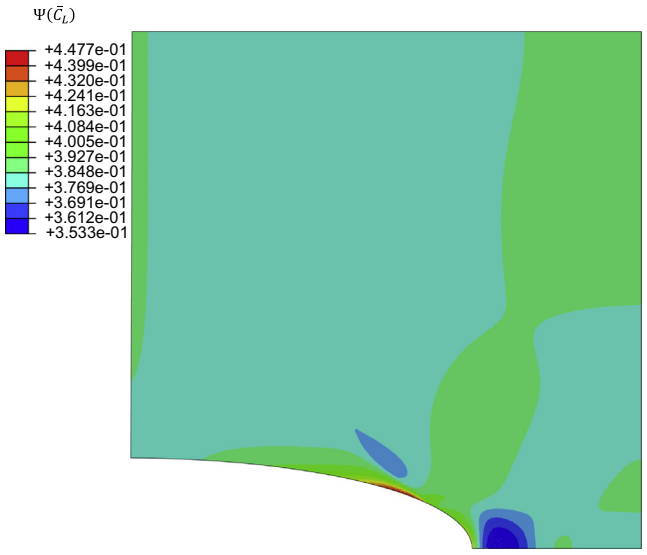

Fig. 8. $\Psi(\bar{C}_L)$ function which dictates how the yield stress varies with $\bar{C}_L$ as shown in Eq. (33).

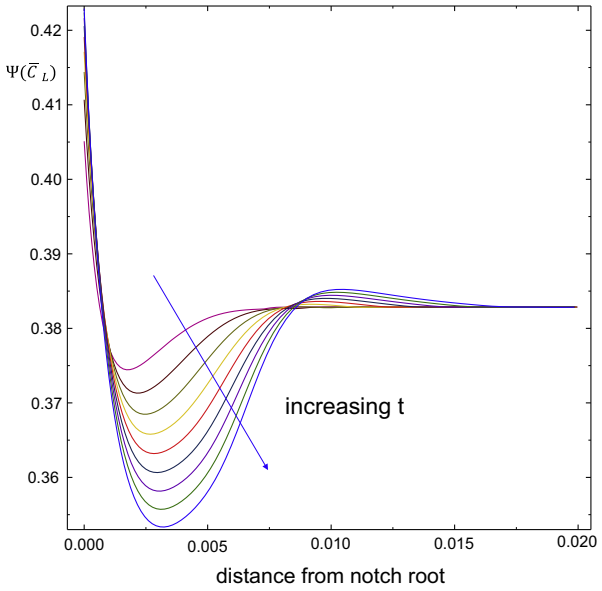

Fig. 9. Distribution of $\Psi(\bar{C}_L)$ ahead of the notch root at different time frames during the simulation.

to material remote from the notch root), the strong kinematic determinacy of this geometry causes the deformation of the material to be the same as for a hardening material, but at a lower local stress level. This results in a local decrease of the hydrostatic as well as effective stress and therefore a lower H concentration. A consequence of this is that the yield strength increases. The net effect here is that the take up of hydrogen and material softening are self regulating processes and a balance is eventually reached, i.e. the deformation does not become unstable with progressive softening of the material. Also, for a plasticity dominated process there must be a global compatible mechanism of localization/collapse. The high kinematic constraint of the component considered here means that there are limited mechanisms of plastic collapse that conserve volume. As a result the deformation is global with significant energy dissipation, i.e. there is no evidence of localization and embrittlement. We have run simulations in which the yield strength hence the $\Psi(\bar{C}_L)$ function decreases more drastically with increasing hydrogen content in the lattice $\bar{C}_L$. In order to achieve this situation we changed the value of $\bar{C}_{min}$ in Eq. (37). We obtain results similar to Fig. 10. There is no evidence of localization of plastic flow and embrittlement. In order for embrittling to occur the HELP mechanism needs to act in synergy with another mechanism such as Hydrogen Induced Decohesion (HID).

Fig. 11 shows the fraction of lattice sites and the fraction of trapping sites occupied by hydrogen. Following Oriani's theory expressed in Eq. (14) θ_X is significantly more sensitive to the binding energy W_B than to $\bar{C}_L$. In Fig. 11(a) $\bar{C}_L$ reaches its max value of $\bar{C}_L = 34.88$ mol m^{-3} which corresponds to $\theta_L = 3.79 \times 10^{-5}$ as

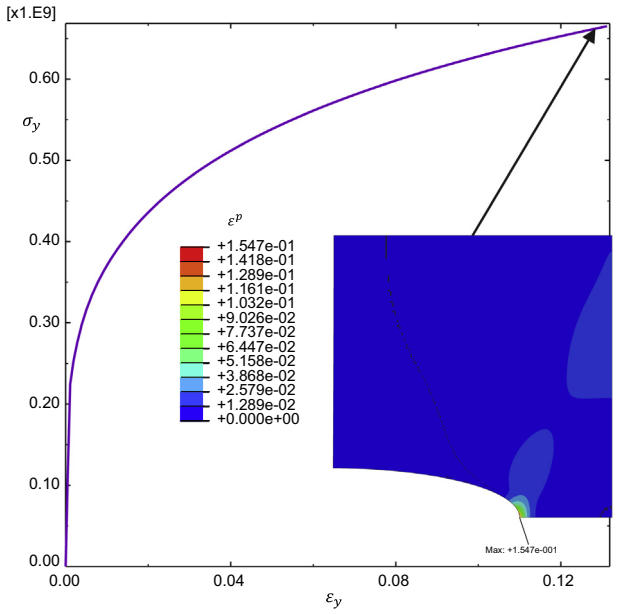

Fig. 10. Stress strain curves $\sigma_0^H = \Psi(\bar{C}_L)\sigma_0$. The distribution of plastic strain at the end of the increment is also included.

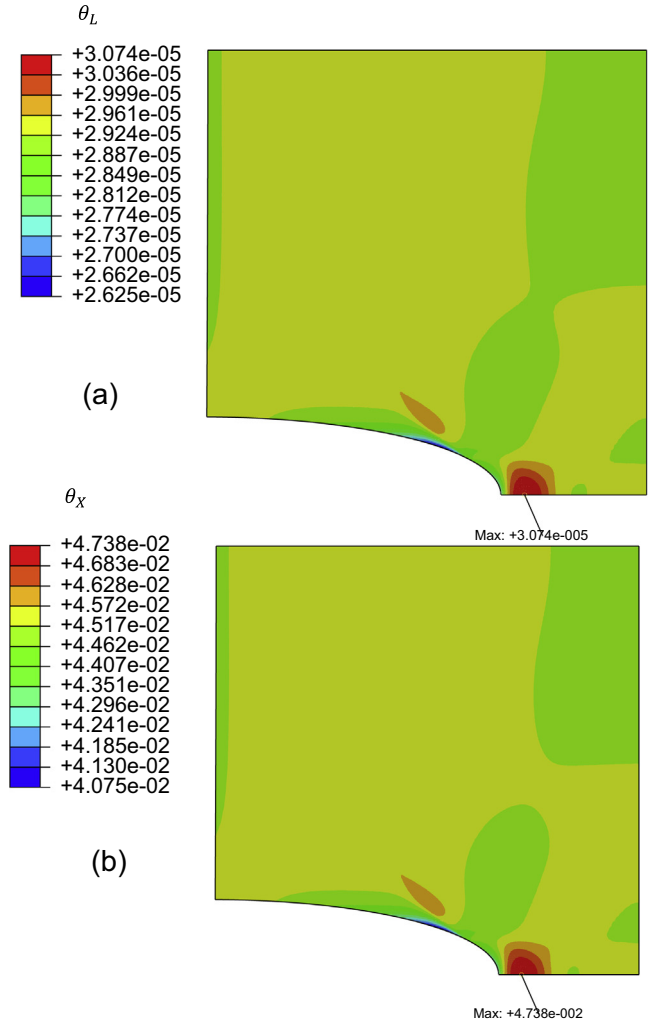

Fig. 11. (a) θ_L fraction of Ni lattice sites occupied by hydrogen. (b) θ_X fraction of trapping (dislocations) sites occupied by hydrogen.

shown in Fig. 11(b). From Fig. 11 the value of $\theta_X = 5.8 \times 10^{-2}$ is about three orders of magnitude higher than θ_L which is consistent with the findings of [23].

5. Discussion and conclusions

The purpose of this paper is to model the HELP (Hydrogen Enhanced Local Plasticity) mechanism, fully coupled with hydrogen transport. The HELP mechanism implies that hydrogen induces material softening at the microscale by reducing the applied stress necessary to move a dislocation through a field of obstacles, hence enhancing dislocation mobility. The two main features of the HELP mechanism are (a) material softening and (b) localization of plastic flow in those regions where the hydrogen content is high. This should lead to an embrittlement of the material. Here the behaviour of the material is represented by an isotropic hardening law in which the flow stress decreases with increasing hydrogen content in the matrix, which is evaluated by solving the fully coupled mechanical-diffusion equations. We assume that hydrogen atoms reside either at NILS or at trapping sites such as dislocations. The presence of plastic strain enhances the dislocation and trap density, i.e. the concentration of hydrogen at dislocation traps which is in equilibrium, following Oriani's theory, with the population of hydrogen at NILS.

We have analysed the response of a plane strain component which contains deep and sharp doubled-edged notches. We observe that (a) hydrogen accumulates in high local hydrostatic stress regions, however high hydrogen concentration results in local softening, i.e. a low yield strength, and therefore a low hydrostatic stress. This is a self-regulating process where a balance between hydrostatic stress, hydrogen concentration and yield strength is achieved. (b) Furthermore we compare the response in the presence and in the absence of hydrogen. The deformation of the component is highly kinematically constrained, resulting in similar strain distribution in both cases. The findings of the simulations reported in this paper show that softening of the constitutive response due to the presence of hydrogen, does not lead to localization of strain and a macroscopic brittle response. In order to observe embrittlement, the HELP mechanism needs to be accompanied by another mechanism such as hydrogen induced decohesion (HID). This is currently being investigated by considering the presence of carbides in the region ahead of the notch. Two effects due to the presence of hydrogen should be considered: (1) the reduction of the yield strength of the material as done in this paper and (2) the reduction of the cohesive strength at the carbide–matrix interface. Decohesion at the carbide/matrix interface and growth of the voids formed around the carbides then promotes localization of plastic flow in regions of high hydrogen concentration ahead of the notch root.

Acknowledgements

O.B and A.C.F.C would like to acknowledge that this work was supported by the Engineering and Physical Sciences Research Council [Programme Grant No. EP/L014742/1]. E.T would like to acknowledge financial support from EPSRC fellowship grant EP/N007239/1. H.W.T wishes to thank the Ministry of Science and Technology of Taiwan, R.O.C., Grant No. NSC 103-2917-I-564-064, and through a National Science Council Overseas Project for Post Graduate Research.

References

[1] T. Scott, A. Troiano, Interstitials and fracture of metals, Nature 185 (4710) (1960) 372–373, http://dx.doi.org/10.1038/185372a0. cited By 2.

[2] H. Johnson, A. Troiano, Crack initiation in hydrogenated steel, Nature 179 (4563) (1957) 777, http://dx.doi.org/10.1038/179777a0. cited By 4.
[3] T. Mohr, A. Troiano, R. Hehemann, Stress corrosion cracking of ferritic stainless steels in chloride solutions, Corrosion 37 (4) (1981) 199–208. cited By 6.
[4] R. Garber, I. Bernstein, A. Thompson, Hydrogen assisted ductile fracture of spheroidized carbon steels, Metall. Trans. A 12 (2) (1981) 225–234, http://dx.doi.org/10.1007/BF02655195. cited By 68.
[5] R. Oriani, P. Josephic, Testing of the decohesion theory of hydrogen-induced crack propagation, Scr. Metall. 6 (8) (1972) 681–688, http://dx.doi.org/10.1016/0036-9748(72)90126-3. cited By 31.
[6] H. Vehoff, W. Rothe, Gaseous hydrogen embrittlement in FeSi- and Ni-single crystals, Acta Metall. 31 (11) (1983) 1781–1793. cited By 70.
[7] I. Robertson, The effect of hydrogen on dislocation dynamics, Eng. Fract. Mech. 64 (5) (1999) 649–673, http://dx.doi.org/10.1016/S0013-7944(99)00094-6. cited By 51.
[8] P. Novak, R. Yuan, B. Somerday, P. Sofronis, R. Ritchie, A statistical, physical-based, micro-mechanical model of hydrogen-induced intergranular fracture in steel, J. Mech. Phys. Solids 58 (2) (2010) 206–226, http://dx.doi.org/10.1016/j.jmps.2009.10.005. cited By 71.
[9] O. Barrera, A. Cocks, Computational modelling of hydrogen embrittlement in welded structures, Phil. Mag. 93 (20) (2013) 2680–2700, http://dx.doi.org/10.1080/14786435.2013.785638. cited By 4.
[10] O. Barrera, A. Cocks, E. Tarleton, Microstructural Image-based Modelling of Weld Failure, 2013, pp. 399–404, cited By 0.
[11] O. Barrera, E. Tarleton, A. Cocks, A micromechanical image-based model for the featureless zone of a Fe–Ni dissimilar weld, Phil. Mag. 94 (12) (2014) 1361–1377, http://dx.doi.org/10.1080/14786435.2014.886023. cited By 1.
[12] A. McNabb, P.K. Foster, A new analysis of the diffusion of hydrogen in iron and ferritic steels, Trans. Met. Soc. AIME 1 (227) (1963) 618–627.
[13] R. Oriani, The diffusion and trapping of hydrogen in steel, Acta Metall. 18 (1) (1970) 147–157, http://dx.doi.org/10.1016/0001-6160(70)90078-7. cited By 646.
[14] P. Sofronis, R.M. McMeeking, Numerical analysis of hydrogen transport near a blunting crack tip, J. Mech. Phys. Solids 37 (3) (1989) 317–350, http://dx.doi.org/10.1016/0022-5096(89)90002-1.
[15] A.H.M. Krom, R.W.J. Koers, A. Bakker, Hydrogen transport near a blunting crack tip, J. Mech. Phys. Solids 47 (4) (1999) 971–992. cited By 119.
[16] E.C. Aifantis, Continuum basis for diffusion in regions with multiple diffusivity, J. Appl. Phys. 50 (3) (1979) 1334–1338, http://dx.doi.org/10.1063/1.326167.
[17] H. Kimizuka, S. Ogata, Slow diffusion of hydrogen at a screw dislocation core in α-iron, Phys. Rev. B – Condens. Matter Mater. Phys. 84 (2) (2011) 1–6, http://dx.doi.org/10.1103/PhysRevB.84.024116.
[18] C. Moriconi, G. Hénaff, D. Halm, Cohesive zone modeling of fatigue crack propagation assisted by gaseous hydrogen in metals, Int. J. Fatigue 68 (2014) 56–66, http://dx.doi.org/10.1016/j.ijfatigue.2014.06.007.
[19] C.-S. Oh, Y.-J. Kim, Coupled analysis of hydrogen transport within abaqus, Trans. Korean Soc. Mech. Eng. A 33 (6) (2009) 600–606, http://dx.doi.org/10.3795/KSME-A.2009.33.6.600. cited By 1.
[20] V.S. Arpaci, Conduction Heat Transfer, Addison-Wesley Pub. Co., Reading, Massachusett, 1966 (Chapter 2).
[21] Y. Liang, P. Sofronis, Micromechanics and numerical modelling of the hydrogen–particle–matrix interactions in nickel-base alloys, Model. Simulat. Mater. Sci. Eng. 11 (4) (2003) 523–551, http://dx.doi.org/10.1088/0965-0393/11/4/308. cited By 26.
[22] P. Sofronis, Y. Liang, N. Aravas, Hydrogen induced shear localization of the plastic flow in metals and alloys, Eur. J. Mech., A/Solids 20 (6) (2001) 857–872.
[23] C. Ayas, V. Deshpande, N. Fleck, A fracture criterion for the notch strength of high strength steels in the presence of hydrogen, J. Mech. Phys. Solids 63 (1) (2014) 80–93, http://dx.doi.org/10.1016/j.jmps.2013.10.002. cited By 3.